

The gluon condensation effect in the cosmic hadron spectra

Wei Zhu¹, Pen Liu¹, Jianhong Ruan¹, Ruiqin Wang² and Fan Wang³

¹Department of Physics, East China Normal University, Shanghai 200241, China

² School of Physics and Physical Engineering, Qufu Normal University, Shandong 273165, China

³Department of Physics, Nanjing University, Nanjing,210093, China

Abstract

Hardening of cosmic proton- and nuclei-spectra is explained by using the gluon condensation (GC) model, which states that a large amount of gluons in proton may condense near the high energy threshold. The results present the GC-effect as common origin of a series of anomalous astrophysical phenomena including the broken power-law in gamma-ray spectra, the excess in positron- and electron-spectra and hardening of proton- and nuclei-spectra.

keywords: cosmic ray theory-gamma ray theory-ultra high energy cosmic rays

1 Introduction

The spectra of cosmic hadrons (pion, nucleon and nuclei) above energy $E \sim 10 GeV$ per nucleon are thought to be the result of acceleration mechanism in supernova remnants (SNRs) and they present a simple power-law except at "knee" ($E \sim 10^3 TeV$) and "ankle" ($E \sim 10^6 TeV$). The power-law of energy spectrum is a general rule of the cosmic-ray (CR) spectra at high energy. It is described by a straight line of the energy spectrum with a fixed index in the double-logarithmic coordinator. However, the precise measurements show that these CR spectra at rigidity $\tilde{R} > 300 GV$ exhibit a remarkable hardening with increasing energies [1]. In particular, proton and helium spectra present an extra peak at $E \sim 11 TeV$.

The origin of the spectral hardening has several explanations: it could be due to the energy dependence of the diffusion coefficient [2,3]; the possible nonlinear acceleration in the source [4,5] and the existence of extra local sources inside SNRs [6,7]. The origin of the CR spectral hardening is still an open question in CR physics [8-10].

The gluons inside proton dominate the proton collisions at high energy and their distributions obey the evolution equations based on Quantum Chromodynamics (QCD). A QCD analysis shows that the evolution equations will become nonlinear due to the initial gluons correlations at high energy and it results in a chaotic solution beginning at a threshold critical energy [11-13]. Most surprisingly, the dramatic chaotic oscillations produce strong shadowing and antishadowing effects, they may converge gluons to a state at a critical momentum. This is the gluon condensation (GC) in proton. In this work we propose that the GC-effect of hadronic collisions in SNR breaks the power-law of the hadron flux and leads to the observed hardening in cosmic hadronic spectra.

The GC means a lot of gluons accumulate at a critical momentum, and the secondary particles are significantly increased near the GC-threshold. Proton-proton (or nucleus-

nucleus) collisions are general events inside SNR, which produce lots of secondary particles (electron-positron, pion, proton-antiproton, nuclei...). Therefore, the GC-effect should induce the characteristic excess in CR spectra originated from $p - p$ collisions, provided the GC-threshold E_{p-p}^{GC} enters the observable high energy region. In our previous work [14] we successfully used the GC-model to explain two seemingly completely different events of the CR spectra: the excess in positron flux and the broken power-law in gamma-ray spectrum of a SNR. We have shown that the excess in the CR positron spectrum observed by AMS originates mainly from the GC-effect in Tycho's supernova remnant. A following naive idea is that the similar excess should also occur in cosmic hadron spectra, since the secondary hadrons are the main products in high energy proton-proton collisions.

We find that the GC-effect may cause a large amount of helium-4 to build up in the formation processes of proton-proton collisions. It directly leads to the excess nucleons and nuclei peaked at $E \sim m_{He}/m_{\pi} \times 400 \text{ GeV} \simeq 11 \text{ TeV}$, 400 GeV is a observed broken point of gamma ray from Tycho's SNR. The GC-effect also predicts that the strength of nuclei fluxes sensitively relates to the average binding energy of the nucleus in the SNR environment. Thus, a series of interesting anomalous power-law show their intrinsic connection through the GC-effect.

We will discuss the properties of the GC effect at Sec.2. Then in Sec. 3 we predict the proton spectrum. Based on the above results, hardening of the cosmic nuclei spectra are studied in Sec. 4. The discussions and a summary are given in Sec. 5.

2 The GC Model

The secondary particles in CRs may origin from the hadronic processes $p(A) + p(A) \rightarrow \pi^\pm + \pi^0 + p + \bar{p} + \text{others}$. Let us first consider a normal high-energy heavy-ions collisions without the GC-effect. It is generally accepted that the partons (quarks and gluons) in the central region of the collision have gone through the following thermalization process: (I) all partons convert to constituent quarks (CQs); (II) all constituent quarks combine to pion, nucleon (proton and neutron), anti-nucleon..., they form a dense and hot hadronic cluster: the fireball; (III) the fireball expands rapidly and the hadron density decreases rapidly. In this cooling process part of nucleons and anti-nucleons may form nuclei and anti-nuclei. That is

$$\begin{aligned}
 & I(G, q\bar{q} \rightarrow CQs) \\
 & \rightarrow II(CQs \rightarrow \pi, p, n\dots) \\
 & \rightarrow III(p, n, \bar{p}, \bar{n} \rightarrow A, \bar{A}).
 \end{aligned} \tag{2.1}$$

Now we consider a high energy collision of heavy ions with the GC-effect inside SNR. One can expect that the CQ cluster will be produced in the central region of the collision as similar to the above normal relativistic heavy ion collision. However, a large number of gluons will be piled in the central region with the collision energy larger than the GC-threshold $E_{A-A} > E_{A-A}^{GC}$. A new research [15,16] found that CQs are formed after bare quark absorbs gluons. Therefore, there are enough CQs to form maximum number of hadrons due to the GC-effect. All available relative kinetic energy of the constituents is almost used to construct the hadrons in the central region. We call it as the cold ball. This assumption described successfully the broken power-law in CR gamma fluxes, if these hadrons are pions [17]. In this work we further consider the contributions of

nucleons and anti-nucleons, which are accompanied by pions in a narrow phase space. In order to get the maximum nucleon occupancy in a small phase space, these nucleons and anti-nucleons should be in the Boson-configuration in the cold ball due to Pauli principle. Helium-4 (4He) and anti-Helium-4 (${}^4\overline{He}$) are the condensable and more stable Bosons comparing with deuteron. Therefore, the cold ball is quite different from the fireball. We have pointed out in our previous paper [17] that $\pi^+ + \pi^- \rightarrow 2\pi^0$ since $m_{\pi^+} + m_{\pi^-} > 2m_{\pi^0}$ and then $\pi^0 \rightarrow 2\gamma$. Thus, there is a large number of photons surrounding 4He , then 4He is quite possible to be dissolved by photons, i.e., ${}^4He(\gamma, D)D$, ${}^4He(\gamma, p)T$ and ${}^4He(\gamma, n){}^3He$. We only consider the first reaction since its product is the Boson-configuration, which can accommodate more hadrons in a small phase space. Thus, we have the following sub-processes ${}^4He \rightarrow D + D$; $D \rightarrow p + n$.

Then part of these dense secondary nucleons and antinucleons recombine light nuclei. Note that most of antinucleons are annihilated by nucleons within SNR, therefore, we don't consider the antiproton spectrum in this report. Besides, the light nuclei with small average binding energy are easily decomposed during collisions. The above descriptions about the cosmic hadron spectra in SNR with the GC-effect can be summarized as the following nuclear reaction chain

$$\begin{aligned}
& I'(\text{condesated } G, q\bar{q} \rightarrow \text{maximum } CQs) \\
& \rightarrow II'(\text{maximun } CQs \rightarrow \text{maximum } \pi^0, {}^4He) \\
& \rightarrow II''(\text{decomposed } {}^4He \text{ by } \gamma \rightarrow \text{dense } p, n, \bar{p}, \bar{n}) \\
& \rightarrow III'(\text{dense } p, n, \bar{p}, \bar{n} \rightarrow A, \bar{A}). \tag{2.2}
\end{aligned}$$

Now we can easily generalize the GC-model for the lepton flux, which has been derived in [14] to include the proton and nuclei fluxes. We denote that $N_\pi(E_{p-p}, E_\pi)$ and

$N_{He}(E_{p-p}, E_{He})$ as π^0 - and 4He -numbers with energies E_π and E_{He} ; E_{p-p} is the energy of incident proton in the rest frame of target. According to the above discussions, we can directly write the relativistic invariant and energy conservation as

$$(2m_p^2 + 2E_{p-p}m_p)^{1/2} \simeq E_{p1}^* + E_{p2}^* + N_\pi m_\pi + N_{He}m_{He}, \quad (2.3)$$

$$E_{p-p} + m_p \simeq m_{p1}\gamma_1 + m_{p2}\gamma_2 + [N_\pi m_\pi + N_{He}m_{He}]\gamma, \quad (2.4)$$

here E_{p1}^* and E_{p2}^* are the energy of the two secondary leading protons in the CM system and we have considered $m_p \ll E_{p-p}$.

Denote

$$E_{He}/E_\pi = E_{He}^{GC}/E_\pi^{GC} = m_{He}/m_\pi \equiv \zeta, \quad (2.5)$$

and

$$N_{He}/N_\pi \equiv \eta \ll 1, \quad (2.6)$$

where we use $\eta = 0.01$ to estimate the ratio of baryon and meson numbers. Note that the value of η is not well defined here. However, its correction to the following parameters in Equations (2.13)-(2.16) can be neglected if η varies over a wide range. We rewrite Equations (2.3) and (2.4) as

$$(2m_p^2 + 2E_{p-p}m_p)^{1/2} = E_{p1}^* + E_{p2}^* + N_\pi m^* \quad (2.7)$$

$$E_{p-p} + m_p = m_{p1}\gamma_1 + m_{p2}\gamma_2 + N_\pi m^* \gamma, \quad (2.8)$$

where $m^* = (1 + \eta\zeta)m_\pi$. We take the inelasticity $K \sim 0.5$ [18] and set

$$E_{p1}^* + E_{p2}^* = \left(\frac{1}{K} - 1\right)N_\pi m^*, \quad (2.9)$$

and

$$m_{p1}\gamma_1 + m_{p2}\gamma_2 = \left(\frac{1}{K} - 1\right)N_\pi m^* \gamma, \quad (2.10)$$

One can get the solutions $N_\pi(E_{p-p}, E_\pi)$ (or $N_{He}(E_{p-p}, E_{He})$) for $p - p$ collisions in the GeV -unit

$$\ln N_\pi = 0.5 \ln E_{p-p(A)} + a_\pi, \quad \ln N_\pi = \ln E_\pi + b_\pi, \quad (2.11)$$

and

$$\ln N_{He} = 0.5 \ln E_{p-p(A)} + a_{He}, \quad \ln N_{He} = \ln E_{He} + b_{He}. \quad (2.12)$$

The parameters a_π , b_π , a_{He} and b_{He} are

$$a_\pi \equiv 0.5 \ln(2m_p) - \ln m^* + \ln K, \quad (2.13)$$

$$b_\pi \equiv \ln(2m_p) - \ln m^* m_\pi + \ln K, \quad (2.14)$$

$$a_{He} \equiv 0.5 \ln(2m_p) - \ln m^* + \ln K + \ln \eta, \quad (2.15)$$

$$b_{He} \equiv \ln(2m_p) - \ln m^* m_{He} + \ln K + \ln \eta. \quad (2.16)$$

Equations (2.11) and (2.12) give the one-to-one relations among N_π , N_{He} and E_{p-p} , which lead to the GC-characteristic spectra.

3 Cosmic proton spectrum

According to the GC-model in Sec.2, cosmic proton flux reads

$$\Phi_p(E) = \Phi_p^0(E) + \Phi_p^{GC}(E), \quad (3.1)$$

where $\Phi_p^0(E)$ is the background spectrum and $\Phi_p^{GC}(E)$ is the GC-contributions through the hadronic chain $p + p \rightarrow {}^4\text{He}$, ${}^4\text{He} \rightarrow 2D$ and $D \rightarrow p + n$,

$$\begin{aligned} \Phi_p^{GC}(E) &= C_p \left(\frac{E}{E_{He}^{GC}} \right)^{-\beta_p} \int_E dE_D \left(\frac{E_D}{E_{He}^{GC}} \right)^{-\beta_D} \int_{E_{He}^{min}}^{E_{He}^{max}} dE_{He} \left(\frac{E_{p-p}}{E_{p-p}^{GC}} \right)^{-\beta_{p'}} \\ &\quad \times N_{He}(E_{p-p}, E_{He}) \frac{d\omega_{He-D}(E_{He}, E_D)}{dE_D} \frac{d\omega_{D-p}(E_D, E)}{dE} \\ &= C_p \left(\frac{E}{E_{He}^{GC}} \right)^{-\beta_p} \int_E \frac{dE_D}{E_D} \left(\frac{E_D}{E_{He}^{GC}} \right)^{-\beta_D} \int_{E_{He}^{GC} \text{ or } E_D}^{E_{He}^{max}} dE_{He} \left(\frac{E_{p-p}}{E_{p-p}^{GC}} \right)^{-\beta_{p'}} N_{He}(E_{p-p}, E_{He}) \frac{2}{\beta_{He} E_{He}} \\ &= \begin{cases} \frac{2C_p e^{b_{He}}}{2\beta_{p'}-1} E_{He}^{GC} \left(\frac{E}{E_{He}^{GC}} \right)^{-\beta_p} \left[\frac{1}{\beta_D} \left(\frac{E}{E_{He}^{GC}} \right)^{-\beta_D} + \left(\frac{1}{\beta_D+2\beta_{p'}-1} - \frac{1}{\beta_D} \right) \right] & \text{if } E \leq E_{He}^{GC} \\ \frac{2C_p e^{b_{He}}}{(2\beta_{p'}-1)(\beta_D+2\beta_{p'}-1)} (E_{He}^{GC}) \left(\frac{E}{E_{He}^{GC}} \right)^{-\beta_p-\beta_D-2\beta_{p'}+1} & \text{if } E > E_{He}^{GC} \end{cases}, \quad (3.2) \end{aligned}$$

where the integral lower-limit takes E_{He}^{GC} (or E_D) if $E_{He} \leq E_{He}^{GC}$ (or if $E_{He} > E_{He}^{GC}$).

$-\beta_p$ is the suppression index of secondary particle p during propagation, and $-\beta_{p'}$ is the index of incident proton which may carry information about their origin. A factor $(E_{He}/E_{He}^{GC})^{-\beta_{He}}$ has been incorporated into $(E_{p-p}/E_{p-p}^{GC})^{-\beta_{p'}}$.

Note that comparing with the high energy E_{p-p} , we neglect the mass of deuterium. After taking average over possible directions of deuterium, the energy distribution of deuterium is equal probability, i.e., the normalized spectrum is

$$\frac{d\omega_{He-D}(E_{He}, E_D)}{dE_D} = \frac{1}{E_{He}}. \quad (3.3)$$

Thus, the processes $p + p \rightarrow He \rightarrow D \rightarrow p + n$ are similar to $p + p \rightarrow \pi^0 \rightarrow \gamma \rightarrow e^+ + e^-$. The later has been discussed as a hadronic mechanism of the positron spectrum in our previous work [17,19], it is written as

$$\begin{aligned}
\Phi_e^{GC}(E) &= C_e \left(\frac{E}{E_\pi^{GC}} \right)^{-\beta_e} \int_E dE_\gamma \left(\frac{E_\gamma}{E_\pi^{GC}} \right)^{-\beta_\gamma} \int_{E_\pi^{min}}^{E_\pi^{max}} dE_\pi \left(\frac{E_{p-p}}{E_{p-p}^{GC}} \right)^{-\beta_p} \\
&\quad \times N_\pi(E_{p-p}, E_\pi) \frac{d\omega_{\pi-\gamma}(E_\pi, E_\gamma)}{dE_\gamma} \frac{d\omega_{\gamma-e}(E_\gamma, E)}{dE} \\
&= C_e \left(\frac{E}{E_\pi^{GC}} \right)^{-\beta_e} \int_E \frac{dE_\gamma}{E_\gamma} \left(\frac{E_\gamma}{E_\pi^{GC}} \right)^{-\beta_\gamma} \int_{E_\pi^{GC} \text{ or } E_\gamma}^{E_\pi^{max}} dE_\pi \left(\frac{E_{p-p}}{E_{p-p}^{GC}} \right)^{-\beta_p} N_\pi(E_{p-p}, E_\pi) \frac{2}{\beta_\pi E_\pi} \\
&= \begin{cases} \frac{2C_e e^{b\pi}}{2\beta_p - 1} E_\pi^{GC} \left(\frac{E}{E_\pi^{GC}} \right)^{-\beta_e} \left[\frac{1}{\beta_\gamma} \left(\frac{E}{E_\pi^{GC}} \right)^{-\beta_\gamma} + \left(\frac{1}{\beta_\gamma + 2\beta_p - 1} - \frac{1}{\beta_\gamma} \right) \right] & \text{if } E \leq E_\pi^{GC} \\ \frac{2C_e e^{b\pi}}{(2\beta_p - 1)(\beta_\gamma + 2\beta_p - 1)} (E_\pi^{GC}) \left(\frac{E}{E_\pi^{GC}} \right)^{-\beta_e - \beta_\gamma - 2\beta_p + 1} & \text{if } E > E_\pi^{GC} \end{cases} \quad (3.4)
\end{aligned}$$

A strong prediction of the GC-model is that the secondary proton and positron spectra are closely related. Equations (3.2) and (3.4) show that the peak positions E_{He}^{GC} and E_π^{GC} of two kinds of spectra are related by equation (2.5), i.e.,

$$E_{He}^{GC} = \frac{m_{He}}{m_\pi} E_\pi^{GC}. \quad (3.5)$$

Besides, $\beta_{p'}$ in Equation (3.2) is equal to β_p in Equation (3.4). The E_{He}^{GC} is fixed to be 10.8 TeV using Equation (3.5) and $\beta_{p'} = 1.4$ in Equation (3.2). Note that we do not investigate the origin of the background, which is taken an extension line in Figure 1 (dashed line). The GC-effect superimposed on the background results a broken power-law in the proton spectrum as shown by solid curve in Fig. 1. The predicted position of an extra peak at $E \sim 10.8 \text{ TeV}$ is consistent with the data. One can find that hardening beginning from kinetic energy $\sim 300 \text{ GeV}/n$ is the slope part of the excess peak due to the GC-effect.

4 Cosmic nuclei spectra

The accelerator experiments show that the production yield of light-nuclei decreases on the order of magnitude as the nuclear mass increment one by one. The production mechanism of light nuclei in the field of heavy-ion physics is one open questions [20]. Normally, the nucleus is randomly combined by nucleons with different distributions in an inflated fireball. Unfortunately, astronomical measurements cannot get these distributions in SRN. We can only use an ideal model to build the formation process of light nuclei at the GC-environment. According to the GC model, all nucleons are closely co-moving with a large common velocity. Although the temperature is very low in the cold ball and the kinetic energy of the nucleon seems not enough to overcome the Coulomb potential, however, the nucleons are closely co-moving, their wave functions have a larger probability of overlap during flight inside a GC-source. We introduce the following simple formula to describe the relation between the detected nuclear flux Φ_A and nucleon flux Φ_p

$$\frac{\Phi_A(E_A)}{\Phi_p(E_p)} = R_A^{A-1}, \quad (4.1)$$

where Φ_A has a same form as Φ_p but $E_A \simeq AE_p$ if neglecting the binding corrections at the recombination process. The parameter R_A is defined as the recombination probability that two nucleons combine to one nucleus. In this work, R_A is a free parameter extracted from data.

Similar to Equation (3.1) we write

$$\Phi_A(E) = \Phi_A^0(E) + \Phi_A^{GC}(E), \quad (4.2)$$

and

$$\Phi_A^{GC}(E) = R_A^{A-1} \Phi_p^{GC}(E). \quad (4.3)$$

That is

$$\Phi_A^{GC}(E) = R_A^{A-1} \times \begin{cases} 3.7 \times 10^{-7} \left(\frac{E}{10800\text{GeV}}\right)^{-1.23} \\ -2.9 \times 10^{-7} \left(\frac{E}{10800\text{GeV}}\right)^{-0.73}, & \text{if } E \leq 10800\text{GeV} \\ 8 \times 10^{-8} \left(\frac{E}{10800\text{GeV}}\right)^{-3.03}, & \text{if } E > 10800\text{GeV}. \end{cases} \quad (4.4)$$

Using the data [21,22] of fluxes for helium and Equation (4.4) we get $R_A = 0.46$ for ${}^4\text{He}$ in Figure 2, where the background is taken as an extension line of Φ_A^0 . Note that the He -flux was then treated as containing only ${}^4\text{He}$ [23].

In the following Figures 3-8, we present the fluxes for lithium, beryllium, boron, carbon, oxygen, nitrogen and oxygen multiplied by $\tilde{R}^{2.75}$ as functions of rigidity \tilde{R} . The relation of kinetic energy per nucleon E_k and rigidity is $E_k = (\sqrt{Z^2\tilde{R}^2 + m_A^2} - m_A)/A$, where m_A is the nuclear mass and Z is the nuclear charge.

The values of R_A are 0.46, 0.14, 0.19, 0.34, 0.51, 0.51 and 0.60 for He, Li, Be, B, C, N and O. Interestingly, the above R_A -order is similar to that of average binding energy of these nuclei (see Figure 9). We suggest that Φ_A will be obviously reduced if the nucleus A has a smaller binding energy, since it is easy to be decomposed during they pass through the matter inside SNR. A smaller binding energy implies a larger decomposition, which corresponding to a smaller value of R_A . Therefore, it is different from Equation (4.1). We cannot record deuterium-, tritium and helium3-fluxes in the CRs at the energy band of the GC-effect since their average binding energies are much smaller than other nuclei. On the other hand, as mentioned in Sec. 2, $\Phi_A \gg \Phi_{\bar{A}}$ for cosmic nuclear fluxes due to strong absorption of the SRN matter.

5 Discussion and summary

Based on a QCD predicted GC-effect, we assume that $p-p$ and $A-A$ collisions produce a lot of hadrons, they fill a limited phase space with the largest number of particles, it forms a cold ball, which is consists of π^0 and 4He . Then 4He again decomposes to nucleons by photons. Part of these nucleons recombine into different light-nuclei according to Equation (4.1). Although there is no direct evidence for the above series of assumptions, the predicted eight spectra in Figures 1-8 can be tested by experiments in the near future.

We emphasize that these nuclei spectra present a series of properties arising from the GC-effect. (i) the extra GC-source in a neighboring SRN produces strong proton and nuclei fluxes, which break the CR power-law; (ii) the peak positions of exceeded hadrons are fixed by Equation (3.5) due to the GC-effect in Equations (2.7) and (2.8); (iii) the GC-effect leads to co-moving nucleons, they are recombined into nuclei according to Equation (4.1).

The GC opens a new window for us to understand a series of anomalous excesses in the high energy CR spectra from the quark-gluon level. Some of the topics is current interests, for example, the typical broken power-law in gamma spectra [17,19], the excess in positron-, electron-spectra [14], even in proton and helium, and the hardening light nuclei-spectra in this work, they may originate from a same basic process: a large amount of gluons may condense near the high energy threshold. Combining Figures 1-8, we predict hardening in a serious of light nuclei spectra. The above anomalous power-law originates from the GC-effect in the nucleon collisions inside SRNs.

The GC-effect forms a new physical state in the universe: high density but cold hadronic cluster, which is quite different from the fireball in heavy ion collision and even in big bang nucleosynthesis (BBN). We think that this is a new field that has not been known to us so far.

In summary, a QCD research predicts that gluons in protons may condensed at a critical momentum in high energy collision of proton-proton. The condensed gluons produce a special hadronic state, in which pion and ${}^4\text{He}$ have high densities. The photons are radiated by neutral pions and decompose helium into nucleons. Part of these nucleons recombine to light nuclei. They are superimposed on the background flux to form hardening in cosmic proton and nuclei spectra. We find that hardening beginning from rigidity $\tilde{R} \sim 300\text{GV}$ is the slope part of the excess peak near $E \sim 11\text{TeV}$ due to the GC-effect. The above explanation is also consistent with the observed the broken power-law in gamma ray spectra of a neighboring SNR and the anomalous excess in CR positron-electron spectra. Because gamma, lepton, nucleon and nuclei are the products of high energy proton-proton collisions and their strength is governed by gluon distribution in the proton, the GC-effect should affect all these spectra with a uniform law. Our results support this prediction.

ACKNOWLEDGMENTS We thank F.L. Shao and J. Song for useful discussions about the recombination mechanism. This work is supported by the National Natural Science of China (No.11851303).

References

- [1] A.A. Lagutin, N.V. Volkov, R.I. Balkin and A.G. Tyumentsev, Origin of hardening and universality of cosmic rays spectra in GV-PV rigidity region, *Journal of Physics: Conf. Series* 1181 (2019) 012023 [astro-ph/1905.06699].
- [2] N. Tomassetti, Propagation of H and He cosmic ray isotopes in the Galaxy: astrophysical and nuclear uncertainties, *Astrophys. and Space Sci.*, 342 (2012) 131.
- [3] Y. Genolini, P.D. Serpico and M. Boudaud et al., Indications for a high-rigidity break in the cosmic-ray diffusion coefficient, *Phys. Rev. Lett.* 119 (2017) 241101 [astro-ph/1706.09812].
- [4] D.C. Ellison, L.O. Drury and J.P. Meyer, Galactic cosmic rays from supernova remnants. II: Shock acceleration of gas and dust, *Astrophys. J.*, 487 (1997) 197.
- [5] V. Ptuskin, V. Zirakashvili and E. S. Seo, Spectra of Cosmic Ray Protons and Helium Produced in Supernova Remnants, *Astrophys. J.*, 763 (2013) 47.
- [6] V. Savchenko, M. Kachelriess and D.V. Semikoz, Imprint of a 2 Million Year old Source on the Cosmic-ray Anisotropy, *Astrophys. J.* 809 (2015) L23.
- [7] M. Kachelriess, A. Neronov and D.V. Semikoz, Signatures of a two million year old supernova in the spectra of cosmic ray protons, antiprotons and positrons, *Phys. Rev. Lett.* 115 (2015) 181103.
- [8] H.S. Ahn, et.al., The Cosmic Ray Energetics And Mass (CREAM) instrument, *Nuclear Instruments and Methods in Physics Research A*, 579 (2007) 1034.
- [9] H.S. Ahn, et. al., Discrepant hardening observed in cosmic-ray elemental spectra, *Astrophys. J.* 714 (2010) L89.

- [10] O. Adriani et al., Measurements of cosmic-ray proton and helium spectra with the PAMELA calorimeter, *Advances in Space Research*, 51 (2013) 219.
- [11] W. Zhu, Z.Q. Shen, J.H. Ruan, Can a Chaotic Solution in the QCD Evolution Equation Restrains High-Energy Collider Physics? *Chin. Phys. Lett.* 25 (2008) 3605.
- [12] W. Zhu, Z.Q. Shen and J.H. Ruan, The chaotic effects in a nonlinear QCD evolution equation, *Nucl. Phys. B* 911 (2016) 1.
- [13] W. Zhu and J.S. Lan, The gluon condensation at high energy hadron collisions, *Nucl. Phys. B* 916 (2017) 647.
- [14] W. Zhu, P. Liu, J.H. Ruan and F. Wang, Possible Evidence for the Gluon Condensation Effect in Cosmic Positron and Gamma-Ray Spectra, *Astrophys. J.* 889 (2020) 127.
- [15] F. Gao, L. Chang, Y.X. Liu, C.D. Roberts and P.C. Tandy, Exposing strangeness: projections for kaon electromagnetic form factors, *Phys. Rev. D* 96 (2017) 034024.
- [16] M. Ding, K. Raya, K. A. Bashir, D. Binosi, L. Chang, M. Chen and C.D. Roberts, $\gamma^* \gamma \rightarrow \eta, \eta'$ transition form factors, *Phys. Rev. D* 99 (2019) 014014.
- [17] W. Zhu, J.S. Lan and J.H. Ruan, The gluon condensation in high energy cosmic rays, *Int. J. Mod. Phys. E* 27 (2018) 1850073.
- [18] T. Gaisser, *Cosmic Rays and Particle Physics* (The Press Syndicate of the University of Cambridge, 1990)
- [19] L. Feng, J.H. Ruan and F. Wang and W. Zhu, Looking for the Gluon Condensation Signature in Protons Using the Earth-limb Gamma-Ray Spectra, *Astrophys. J.* 868 (2018) 2.

- [20] S. Hornung, (on behalf of the ALICE Collaboration), (Anti-)nuclei production and flow in pp, p–Pb and Pb–Pb collisions with ALICE, arViv:nucl-ex:1910.00438.
- [21] Y.S. Yoon, et. al., Proton and Helium Spectra from the CREAM-III Flight, *Astrophys. J.* 839 (2017) 5.
- [22] V. Derbina, et. al., Cosmic-ray spectra and composition in the energy range of 10-TeV - 1000-TeV per particle obtained by the RUNJOB experiment, *Astrophys. J.* 628 (2005) L41.
- [23] M. Aguilar, et. al., Precision Measurement of the Helium Flux in Primary Cosmic Rays of Rigidities 1.9 GV to 3 TV with the Alpha Magnetic Spectrometer on the International Space Station, *Phys. Rev. Lett.* 115 (2015) 211101.
- [24] M. Aguilar, et. al., Precision Measurement of the Proton Flux in Primary Cosmic Rays from Rigidity 1 GV to 1.8 TV with the Alpha Magnetic Spectrometer on the International Space Station, *Phys. Rev. Lett.* 114 (2015) 171103.
- [25] M. Aguilar, et. al., Observation of the Identical Rigidity Dependence of He, C, and O Cosmic Rays at High Rigidities by the Alpha Magnetic Spectrometer on the International Space Station, *Phys. Rev. Lett.* 119 (2017) 251101.
- [26] A.D. Panov, et. al., Energy Spectra of Abundant Nuclei of Primary Cosmic Rays from the Data of ATIC-2 Experiment: Final Results, *Physics*, 73 (2009) 564.
- [27] M.J.Christ et. al., Cosmic-ray proton and helium spectra: Results from the JACEE Experiment, *Astrophys. J.* 502 (1998) 278.
- [28] A.D. Benedittis, (on behalf of the DAMPE Collaboration), Proton energy spectrum with the DAMPE experiment, *EPJ Web of Conferences* 209 (2019) 01030.

- [29] M. Aguilar, et. al., 2018, Observation of Fine Time Structures in the Cosmic Proton and Helium Fluxes with the Alpha Magnetic Spectrometer on the International Space Station, Phys. Rev. Lett. 121 (2018) 051101.

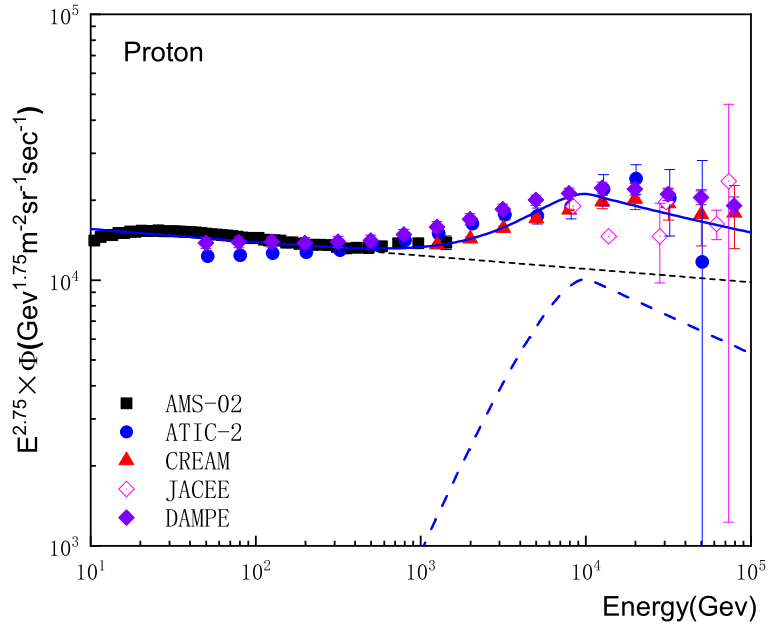


Figure 1: The proton energy spectrum multiplied by $E^{2.75}$ as function of proton energy (solid curve). The dotted curve is background. The GC-contributions (dashed curve) are predicted by Equation (3.2). Note that the peak position of proton flux is fixed by that of positron flux and Equation (3.5). The used parameters are $\beta_p = 0.73$, $\beta_D = 0.5$ and $C_p = 1.55 \times 10^{-11} (GeV^{-3} \cdot m^{-2} \cdot sr^{-1} \cdot sec^{-1})$. The position of the peak E_{He}^{GC} in Equation (3.2) is fixed by the positron spectrum. The data are taken from AMS [24,25], ATIC [26], CREAM [21], JACEE [27], RUNJOB [22] and DAMPE [28].

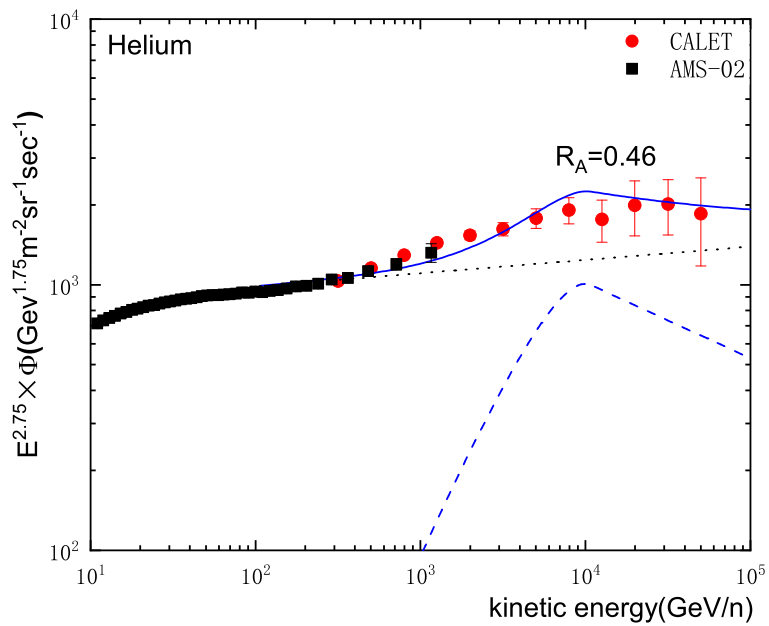


Figure 2: The helium energy spectrum multiplied by $E^{2.75}$ as function of proton energy (solid curve). The dotted curve is background. The GC-contributions (dashed curve) are predicted by Equation (4.4). The E_k position of the peak is fixed by the positron spectrum. A free parameter $R_A = 0.46$. The data are taken from AMS-02 [25] and CREAM [21].

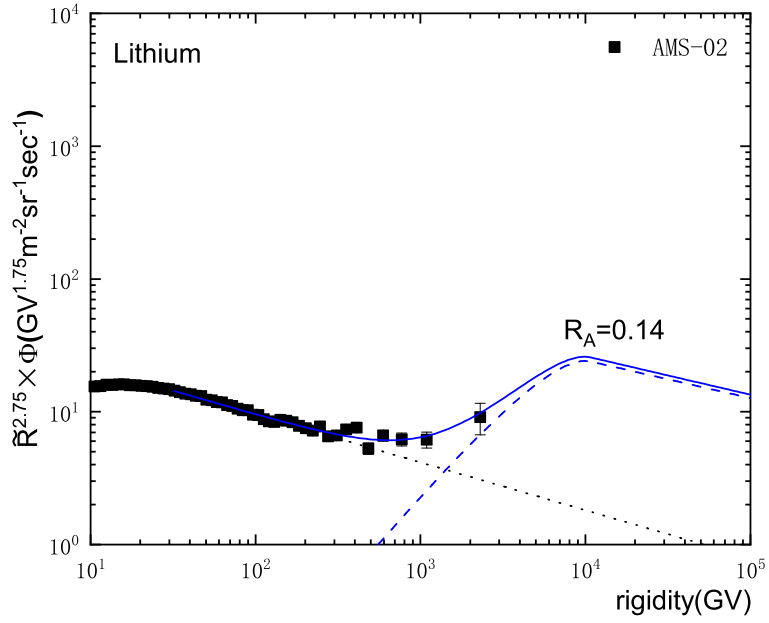


Figure 3: The lithium energy spectrum multiplied by $\tilde{R}^{2.75}$ as function of rigidity (solid curve). The dotted curve is background. The GC-contributions (dashed curve) are predicted by Equation (4.4). The \tilde{R} position of the peak is fixed by the positron spectrum. A free parameter $R_A = 0.14$. Data are taken from the AMS-02 [29].

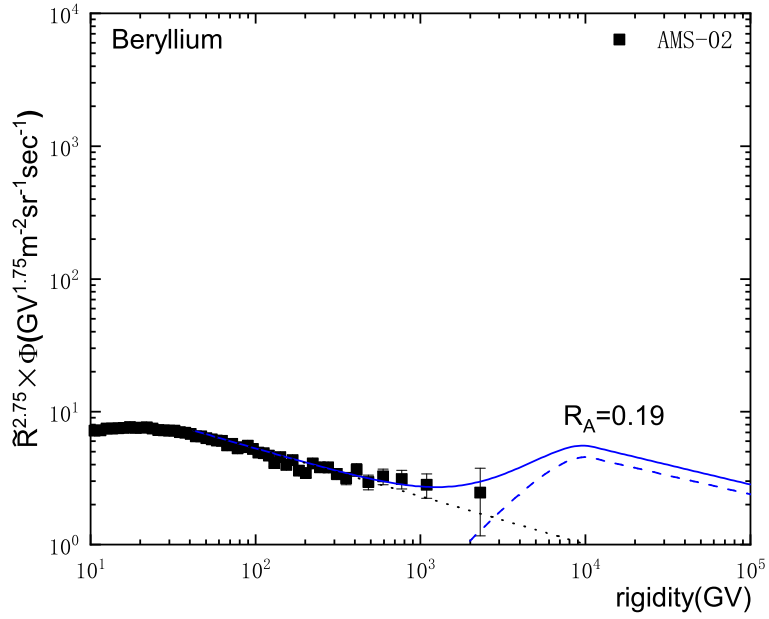


Figure 4: The beryllium energy spectrum multiplied by $\tilde{R}^{2.75}$ as function of rigidity (solid curve). The dotted curve is background. The GC-contributions (dashed curve) are predicted by Equation (4.4). The \tilde{R} position of the peak is fixed by the positron spectrum. A free parameter $R_A = 0.19$. Data are taken from the AMS-02 [29].

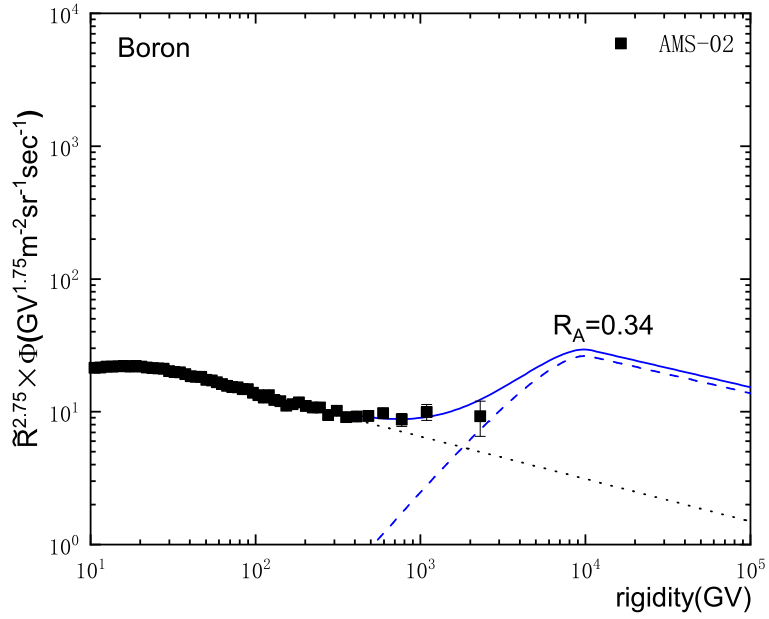


Figure 5: The boron energy spectrum multiplied by $\tilde{R}^{2.75}$ as function of rigidity (solid curve). The dotted curve is background. The GC-contributions (dashed curve) are predicted by Equation (4.4). The \tilde{R} position of the peak is fixed by the positron spectrum. A free parameter $R_A = 0.34$. Data are taken from the AMS-02 [29].

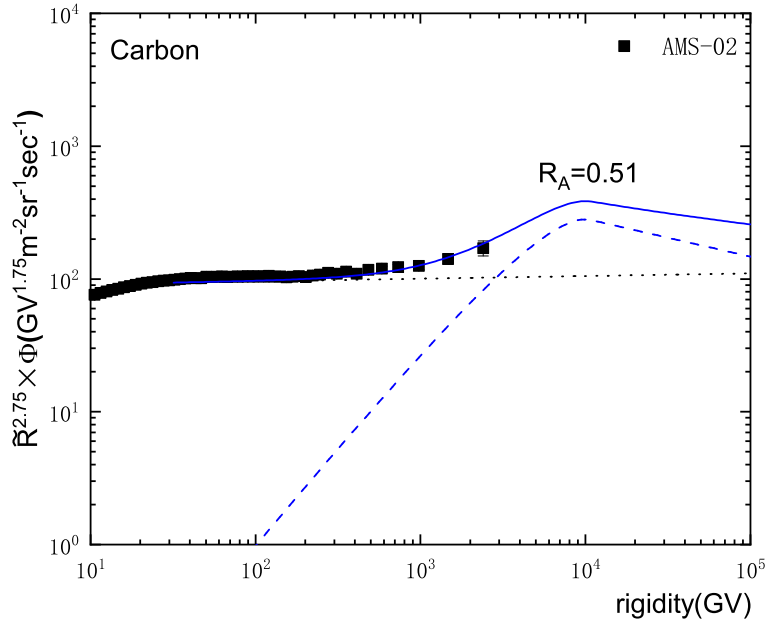


Figure 6: The carbon energy spectrum multiplied by $\tilde{R}^{2.75}$ as function of rigidity (solid curve). The dotted curve is background. The GC-contributions (dashed curve) are predicted by Equation (4.4). The \tilde{R} position of the peak is fixed by the positron spectrum. A free parameter $R_A = 0.51$. Data are taken from the AMS-02 [29].

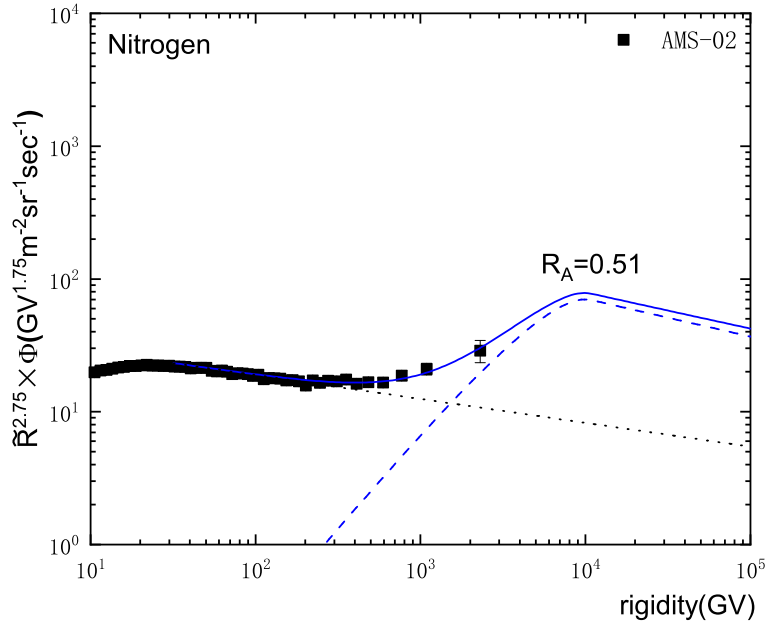


Figure 7: The nitrogen energy spectrum multiplied by $\tilde{R}^{2.75}$ as function of rigidity (solid curve). The dotted curve is background. The GC-contributions (dashed curve) are predicted by Equation (4.4). The \tilde{R} position of the peak is fixed by the positron spectrum. A free parameter $R_A = 0.51$. Data are taken from the AMS-02 [29].

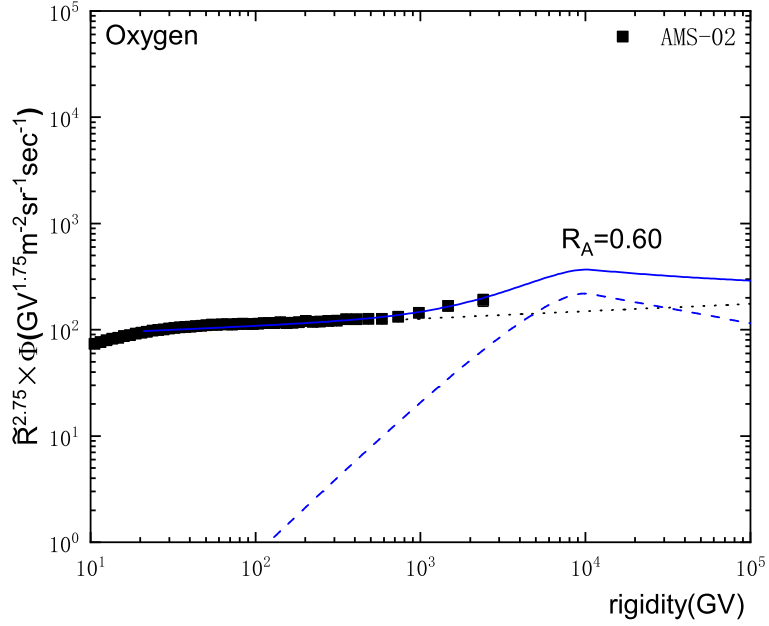


Figure 8: The oxygen energy spectrum multiplied by $\tilde{R}^{2.75}$ as function of rigidity (solid curve). The dotted curve is background. The GC-contributions (dashed curve) are predicted by Equation (4.4). The position \tilde{R} of the peak is fixed by the positron spectrum. A free parameter $R_A = 0.60$. Data are taken from the AMS-02 [29].

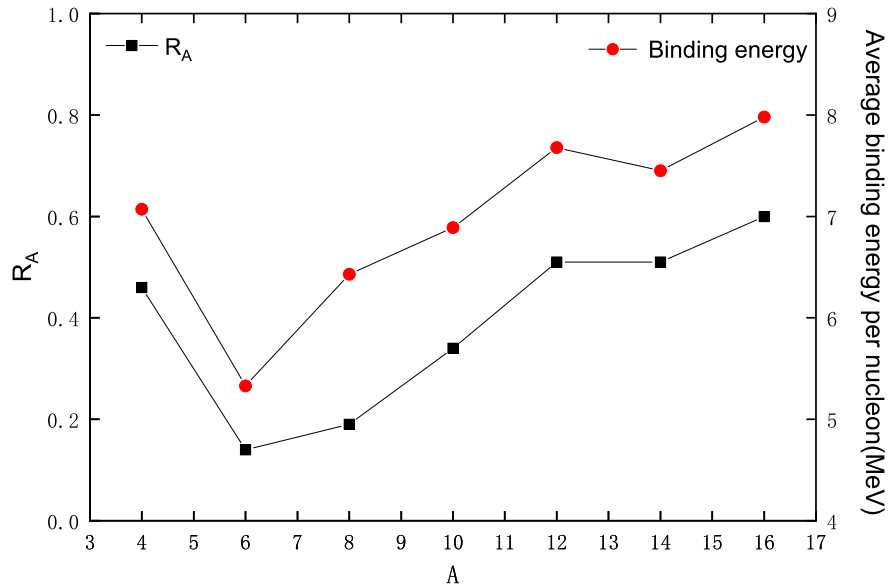


Figure 9: Values of parameter R_A in Equation (4.5) for He, Li, Be, B, C, N and O, and corresponding average binding energy per nucleon.